CHEMICAL VAPOR DEPOSITION

RECENT ADVANCES AND APPLICATIONS IN OPTICAL, SOLAR CELLS AND SOLID STATE DEVICES

Edited by **Sudheer Neralla**

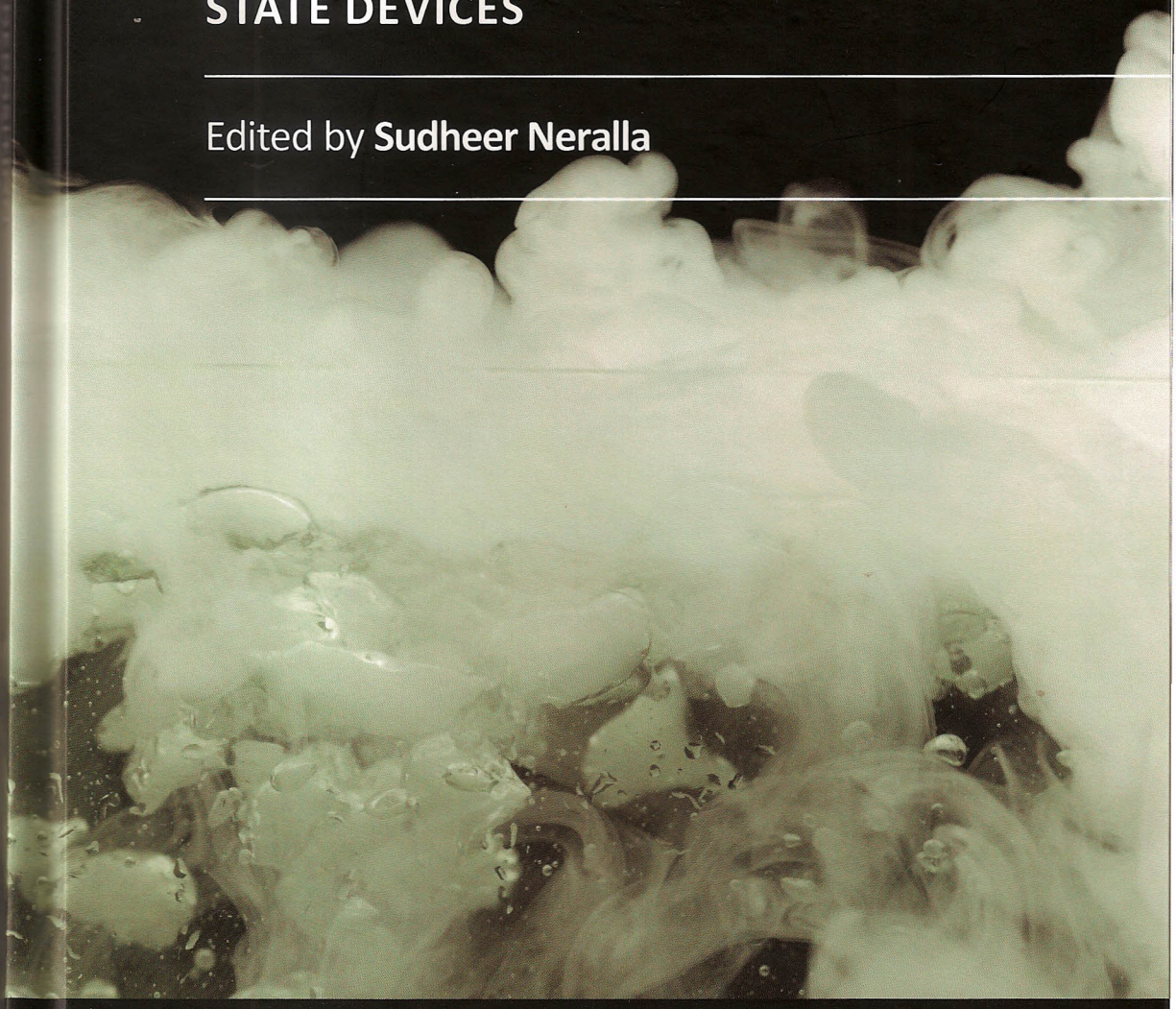

INTECH

Chemical Vapor Deposition - Recent Advances and Applications in Optical, Solar Cells and Solid State Devices
http://dx.doi.org/10.5772/61559
Edited by Sudheer Neralla

Contributors

Hitoshi Habuka, Chang-Seop Lee, Yura Hyun, Aide Torres-Huerta, Pawel Madejczyk, Frank Mendoza, Tej Limbu, Brad Weiner, Gerardo Morell, Milana Vasudev, Haiping Zhou, Shuyan Xu, Shaoqing Xiao, J. Alarcón-Salazar, R. López-Estopier, E. Quiroga-González, A. Morales-Sánchez, J. Pedraza-Chávez, Mariano Aceves-Mijares, Ignacio Enrique Zaldivar Huerta, Nong Moon Hwang, Vahid Mohammadi, Stoyan Nihtianov

Published by InTech

Janeza Trdine 9, 51000 Rijeka, Croatia

Notice

Statements and opinions expressed in the chapters are these of the individual contributors and not necessarily those of the editors or publisher. No responsibility is accepted for the accuracy of information contained in the published chapters. The publisher assumes no responsibility for any damage or injury to persons or property arising out of the use of any materials, instructions, methods or ideas contained in the book.

Publishing Process Manager Edi Lipovic

Technical Editor SPi Global

Cover InTech Design team

First published August, 2016

Printed in Croatia

Additional hard copies can be obtained from orders@intechopen.com

Chemical Vapor Deposition - Recent Advances and Applications in Optical, Solar Cells and Solid State Devices, Edited by Sudheer Neralla

p. cm.

Print ISBN 978-953-51-2572-3
Online ISBN 978-953-51-2573-0

Chapter 7

Silicon-Rich Oxide Obtained by Low-Pressure Chemical Vapor Deposition to Develop Silicon Light Sources

J. Alarcón-Salazar, R. López-Estopier, E. Quiroga-González, A. Morales-Sánchez, J. Pedraza-Chávez, I. E. Zaldívar-Huerta and M. Aceves-Mijares

Additional information is available at the end of the chapter

http://dx.doi.org/10.5772/63012

Abstract

Off stoichiometric silicon oxide, also known as silicon-rich oxide (SRO), is a light-emitting material that is compatible with silicon technology; therefore, it is a good candidate to be used as a light source in all-silicon optoelectronic circuits. The SRO obtained by low-pressure chemical vapor deposition (LPCVD) has shown the best luminescent properties compared to other techniques. In spite of LPCVD being a simple technique, it is not a simple task to obtain SRO with exact silicon excess in a reliable and repetitive way. In this work, the expertise obtained in our group to obtain SRO by LPCVD with precise variation is presented. Also, the characteristics of this SRO obtained in our group are revised and discussed. It is demonstrated that LPCVD is an excellent technique to obtain single layers and multilayers of nanometric single layers with good characteristics.

Keywords: SRO, LPCVD, photoluminescence, electroluminescence, multilayer

1. Introduction

Chemical vapor deposition (CVD) is a versatile and economical technique used to deposit different materials. In the microelectronics industry, it has found a main place and it is a standard process. Currently, many efforts are being done to produce optoelectronic circuits using the mature technology of integrated circuits. A major drawback to integrate a whole

silicon circuit that manages both electronic and optical signals is that silicon does not emit light efficiently. There are serious restrictions to integrate a light source in such a system [1]. Basically, two approaches have been under study to solve the problem of the light source: One of them uses a reverse-biased *pn* junction [2], the other one uses light-emitting materials that are compatible with silicon [3, 4]. In spite of the fact that both approaches have shown that it is possible to integrate a complete optoelectronic system based on Si, there is still a wide field of possibilities to improve the efficiency of the light emitters [2, 5], and in consequence, of the whole system.

Off stoichiometric silicon oxide (with empirical formula SiO_x), also known as silicon-rich oxide (SRO), is a good material to be used as a light source in all-silicon optoelectronics circuit [6]. It is obtained by different techniques, including plasma-enhanced and low-pressure chemical vapor deposition (PECVD and LPCVD) methods. The silicon excess in SRO obtained by LPCVD can be easily controlled during the deposition by the ratio of the reactive gases, in our case silane and nitrous oxide:

$$R_0 = \frac{P_{N_2O}}{P_{SiH_4}} \tag{1}$$

Dong et al. showed that for R_0 = 10, 20, and 30, the corresponding silicon excess is about 12, 7 and 5 at %, respectively; that is, SiO_x with x = 1.13, 1.50, and 1.63 [7]. However, it is worthy to mention that SiO_x is a multiphase material composed of SiO_2, elemental silicon, and SiO_y. Thus, SiO_x is an empirical formula to denote SRO (which may contain large Si excess), and SiO_y is an oxide with stoichiometry deviating a bit from SiO_2. Oxidation states obtained by X-ray photoelectron spectroscopy (XPS) of LPCVD-SRO for R_0 =10, 20, and 30 are shown in [4]. Depending on the silicon excess, SRO has different characteristics: For low silicon excess, the density of SiO_y compounds dominates, producing intense luminescence. However, for high silicon excess the density of elemental silicon increases, what reduces the emission, but increases the conductivity of the films.

In order to have intense luminescent SiO_x, high-temperature treatments are required. For SRO obtained using LPCVD, 1100°C in nitrogen is the most favorable temperature. Additionally, the emission also depends on the R_0. The emission increases as R_0 increases, being R_0 = 30 the top one; for R_0 higher than 30, the emission reduces again. On the other hand, the conductivity increases as the R_0 reduces, This compromise is important when electroluminescent devices are the goal. Therefore, structures that combine layers of high conductivity with layer of high emission properties are under study to obtain efficient light sources compatible with silicon.

SRO obtained using LPCVD is perhaps the most luminescent compared with SRO obtained by other methods [6]; however, in this technique, it is difficult to control the silicon excess with some precision, and to have films with controllable properties required of personal with expertise on this type of technique.

http://dx.doi.org/10.5772/63012

In this paper, details of our LPCVD deposition processes to obtain SRO single layers (SLs) and multilayers (MLs) with different R_0, including details of our LPCVD system, are described. Also, the optical and structural characteristics of our SRO layers and multilayers are reviewed. Electroluminescence (EL), cathodoluminescence (CL), and photoluminescence (PL) results will be presented and discussed.

2. Our system

We have two homemade LPCVD reactors, one for two- and another for four-inch wafers. Both reactors have the same layout, thus we will describe only one of them in a general way. Our laboratory is a teaching and research facility, therefore every day different materials have to be deposited and the equipment has to be very versatile. For this reason, we found that controlling it manually produces better results than using automatic parts, then the control of the gas flux using rotameter (ABB model 10A6131NB1B1X00) give us enough functionality. High throughput is not required and our main concern is to have good films with repetitive characteristics. Normally, polysilicon, silicon nitride, silicon oxynitride, and SROs are deposited in the reactor; however, we are not limited to only those materials. Perhaps, obtaining SROs with good characteristics is the most demanding, that is because small differences in silicon excess produce big changes in its characteristics. In the following paragraphs, we will concentrate on describing the details to obtain SRO in a controllable manner.

As shown in **Figure 1**, our LPCVD system is hot wall type that allows having a uniform temperature in the whole deposition chamber area. The heating element is a three-zone furnace, and a flat zone of ±2°C can be obtained. In the past, an analysis using multivariated experiment was carried out to study different parameters involved in the deposition process [8]. Based on that, we decide to maintain the wafer horizontally on a flat quartz wafer holder. The working temperature profile was chosen with an increasing slop to obtain lesser thickness variation, as shown in **Figure 2**. The increasing temperature compensates the changes of the boundary layer and produces a more uniform deposition through the flat wafer holder [9]. The deposition temperature allows to deposit SRO from $R_0 = 5$ to $R_0 = 100$.

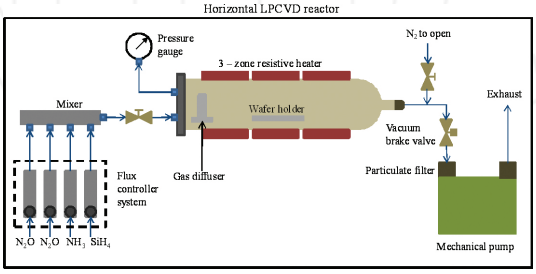

Figure 1. Schematic of the LPCVD system. A three zones furnace and mechanical pump are used.

To obtain SRO, the reactive gases are N_2O and SiH_4 at 5%, the silane is diluted in N_2. The high dilution of silane is a restriction of the system in order to increase the versatility of the reactor. Thereby, we have no possibilities to vary the chamber pressure varying a gas carrier. **Figure 3** shows a calibration graph of the pressure of silane and nitrous oxide as a function of the gas flux. The flux of the N_2O is controlled by two rotameters as shown in the schematic of **Figure 1**. Double control of nitrous oxide allows for an efficient way to produce nanometric layers in multilayers with different R_0, that is, layers of different silicon excess. For the two previous figures, the vacuum valve was 75% open and the base vacuum was at least 6 mTorr.

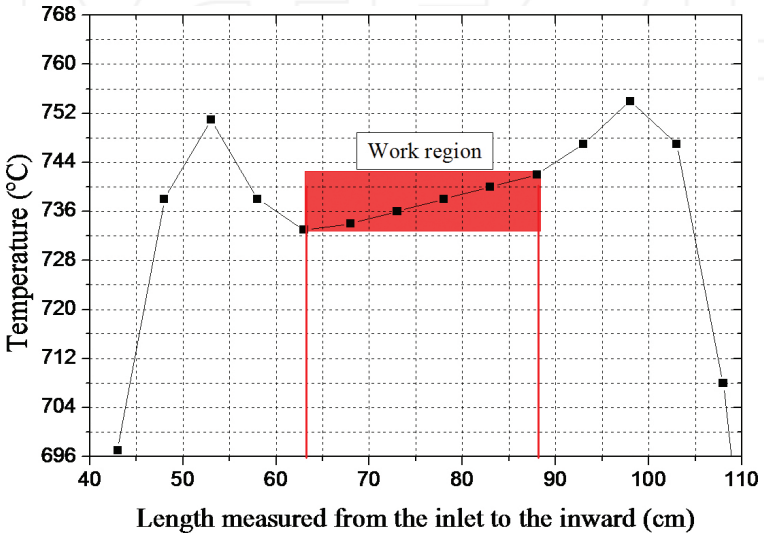

Figure 2. Working temperature profile to deposit SRO with different R_0´s. The profile increases along the deposit area to compensate for the boundary layer.

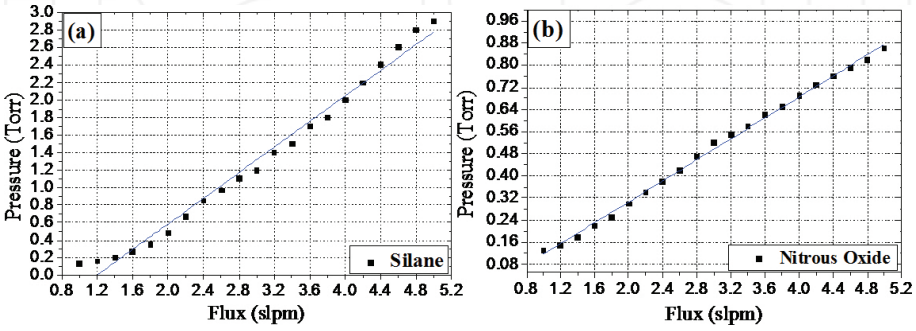

Figure 3. Calibration graph of pressure as function of the gas flux of (a) silane and (b) nitrous oxide. In case of N_2O, the flux is controlled by two rotameters.

http://dx.doi.org/10.5772/63012

The characteristics of the SRO depend strongly on the silicon excess; the flux ratio R_0 is used to control such excess. In the LPCVD technique, it is easy controlling the R_0 by the ratio of partial pressure of each gas, defined in Eq. (1). In our case, the dilution of silane has to be taken into account. Therefore, Eq. (1) has to be written adding a multiplying factor (F) as

$$R_0 = \frac{P * P_{N_2O}}{P_{SiH_4}} \tag{2}$$

Considering that only 0.05 parts of gas corresponds to silane, F takes a value equal to 20. However, due to the natural variation of the gas provided by the supplier, when a new tank is used, a new calibration is carried out in such a way that the refractive index (n) and PL are kept within the known values. Then, normally, the multiplicative factor is different than 20. This procedure is also done periodically to assure the gases aging do not alter the characteristics of the SRO films.

In the everyday procedure to obtain always the same conditions, we fixed the P_{SiH4} and varied the P_{N2O} as required by the R_0; **Table 1** shows the set values used for different R_0. To deposit single layers, the flux of silane is varied until the partial pressure is obtained, then the silane valve is closed and the nitrous oxide flux is set until the partial pressure is obtained. Next, both valves are shutoff and wafers are loaded. When the base vacuum is established, silane and nitrous oxide valves are simultaneously opened. The reactive gases mix and react producing variations in pump extraction and a reduction of the total pressure is observed. That is, the total pressure is different from that of the sum of the partial pressures. Also, a variation of the gases flux is observed. To obtain a repetitive process, it is necessary to adjust the fluxes to the values they had before the gases are mixed. This procedure assures to obtain repeatable characteristics. Also in **Table 1**, the refractive index, the rate of deposition, and the thickness variation from beginning to end of the wafer holder are presented.

R_0	Silane (SiH_4)		Nitrous oxide (N_2O)		Deposit rate (nm/min)	Refractive index	Thickness variation (%)
	P (Torr)	Flux (slpm)	*P* (Torr)	Flux (slpm)			
5	0.97	2.6	0.20	1.5	7.10	2.742	–
10			0.30	2.0	5.20	1.74 ± 0.05	13
20			0.60	3.4	3.80	1.64 ± 0.03	3
25			0.74	4.5	3.10	1.57 ± 0.01	2
30			0.88	5.2	3.05	1.52 ± 0.01	2
50			1.5	9.8	6.50	1.44 ± 0.01	12

Table 1. Deposit conditions in LPCVD system for different R_0's, also the refractive index, the deposit rate and the thickness variation is presented.

There are many partial pressures combinations that fulfill Eq. (1). However, depending on each laboratory conditions, it is recommendable to set a linear relationship between the flux ratio and the partial pressure ratio of each R_0. In our knowledge, it is very important to maintain a linear relationship of the ratios of pressure and flux (**Figure 4**) between the different R_0's. Nevertheless, different deposit conditions such as pump valve aperture, system cleanliness, dilution of silane, and aging produce different relations. In our experiments, all the mentioned factors were taken into account varying the multiplicative factor (F) of Eq. (2). **Figure 4** shows different relationship varying the F due to different conditions of the system. In our system, using the vacuum valve open at 75% of the maximum aperture and purging with nitrogen the gas lines a couple of hour before the deposit are enough to maintain a linear relationship, and with it we obtain repetitive results.

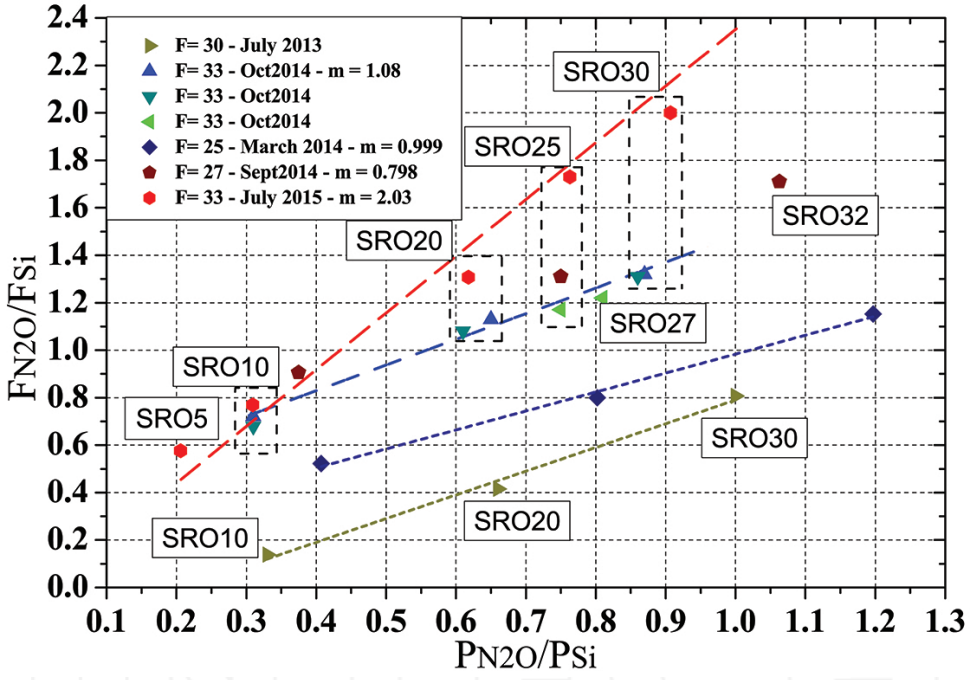

Figure 4. Linear relationship between flux ratio and partial pressure ratio of each R_0.

To deposit a multilayer with different R_0's, the procedure is similar to that of single layers. However, in this case, the flux of N_2O is set using the two flux controls. Using the gas that goes through one of them, one R_0 is fixed (Ro1). The other R_0 (Ro2) is fixed by using the second rotameter or both simultaneously, depending on the deposit conditions. The nitrous oxide valves are open during the time needed to obtain the Ro1 or Ro2 successively. The time required for each layer is established to have the nominal thickness, and it is calculated from the rate of deposit. If the layer being deposited is thin, then the time can be some seconds.

http://dx.doi.org/10.5772/63012

As it is expected in a low-pressure system, deposition in our system works under surface reaction kinetics limited [9, 10]. It implies that the deposit rate is low and good step coverage is obtained, and also by-products are trapped in the film, and that is why off stoichiometric silicon oxide is obtained. The LPCVD also has shown good step coverage, and in order to corroborate our step coverage results, the sticking factor and the gas arrival dates are estimated.

The sticking coefficient (S) is defined as

$$S = \frac{R_r}{A_r} \tag{3}$$

where R_r is the reaction rate and A_r is the arrival rate, respectively. The reaction rate is related with deposit rate; meanwhile the arrival rate is the velocity of the total flux of precursor gases that enters into the chamber. In our case, A_r is estimated as

$$A_r = \frac{F_T}{A} \tag{4}$$

where F_T is the sum of the fluxes of precursor gasses and A is the tubing area (our system uses ¼ inches diameter). Using Eqs. (3) and (4) and conditions from **Table 1**, the sticking coefficient is determined for each R_0. **Table 2** shows results of A_r, R_r, and S for each R_0 from 5 to 50. The sticking coefficient has values in the order to 10^{-11}. This value is rather too low; however, independent of the numerical value, it agrees with what is expected from a low-pressure system; see, for example, [9–11].

R_0	A_r (m/min)	R_r (m/min)	S
5	32.36	7.10E-09	5.48E-11
10	36.31	5.20E-09	3.58E-11
20	47.36	3.80E-09	2.01E-11
25	56.04	3.10E-09	1.38E-11
30	61.57	3.05E-09	1.24E-11
50	97.88	6.50E-09	1.66E-11

Table 2. Arrival and reaction rates and sticking coefficient for SRO-LPCVD deposited at 736°C.

3. Experimental procedure

SRO films were deposited on <100> and low resistivity (5–10 Ω cm) silicon substrates by LPCVD at 736°C. The ratio between reactive gases nitrous oxide (N_2O) and silane (SiH_4) was

varied to obtain films with different silicon excess. Single layers with R_0 values of 5, 10, 20, 25, 30, 35, and 50 were deposited, and will be labeled as SRO_5, SRO_{10}, SRO_{20}, SRO_{25}, SRO_{30}, SRO_{35}, and SRO_{50}, respectively, for clarity. Also, two multilayer structures were fabricated. The multilayer is a stack of seven layers. One structure intercalates three SRO_{25} layers with four SRO_5 layers, and the second one with four SRO_{10} layers. After deposition, all samples were thermally annealed at 1100°C for 3 h in nitrogen ambience to induce the silicon agglomeration.

Thickness and refractive index of all samples, including multilayer structure, were determined using a null ellipsometer Gaertner L117 with a laser He–Ne of 632.8 nm wavelength. The PL emission spectra were obtained with a Fluoromax-3 spectrometer; all the films were excited with UV radiation (300 nm) and the luminescence was measured from 370 to 1000 nm with a resolution of 1 nm. Optical filters were used in order to guarantee the wavelength of excitation beam. CL measurements were performed using a luminoscope equipment model ELM2-144, 0.3-mA current and 5 kV were used. The luminescence spectra (PL and CL) were measured at room temperature.

For electrical and electroluminescent studies, Metal-Insulator-Semiconductor (MIS) devices were fabricated, and we refer to them as light emitting capacitor (LEC). A ~250-nm-thick semitransparent n^+ polycrystalline silicon (Poly) gate was deposited onto the SRO film surface by LPCVD. After a photolithography process step, square-shaped gates of 4-mm^2 area were defined. The backside contact was formed with 1-μm thick aluminum layer by evaporation. Finally, the devices were thermally annealed at 480°C in forming gas.

A source meter Keithley model 2400 was used to obtain current versus voltage (I-V) curves. EL spectra were obtained by biasing the device with a constant DC voltage. The light emitted was collected with an optical fiber located facing the Poly gate and connected to the Fluoromax 3 spectrometer.

4. Composition of SRO by LPCVD

SRO is a multiphase material composed of silicon oxides of different stoichiometry and Si nanocrystals (Si-ncs). In XPS spectra of this material, each Si 2p core level band is composed of bands originated in Si at different oxidation states (Si^0, Si^{1+}, Si^{2+}, Si^{3+}, Si^{4+}), which manifest themselves at different energies. The position of the peaks corresponding to Si^0 and Si^{4+} (SiO_2) is well known and is easily distinguishable [12], but the peaks related with silicon suboxides cannot be distinguished unequivocally in a complex spectrum composed of different Si oxide species; they have been usually studied at Si/SiO_2 interfaces [13–16]. In this way, a quantitative analysis of such highly convoluted spectra is not straightforward. The material can be conveniently considered as composed of SiO_2, elemental Si and SiO_y with $0 < y < 2$. **Figure 5** shows an XPS spectrum of SRO with $R_0 = 1$ as example. The three phases can be clearly distinguished.

http://dx.doi.org/10.5772/63012

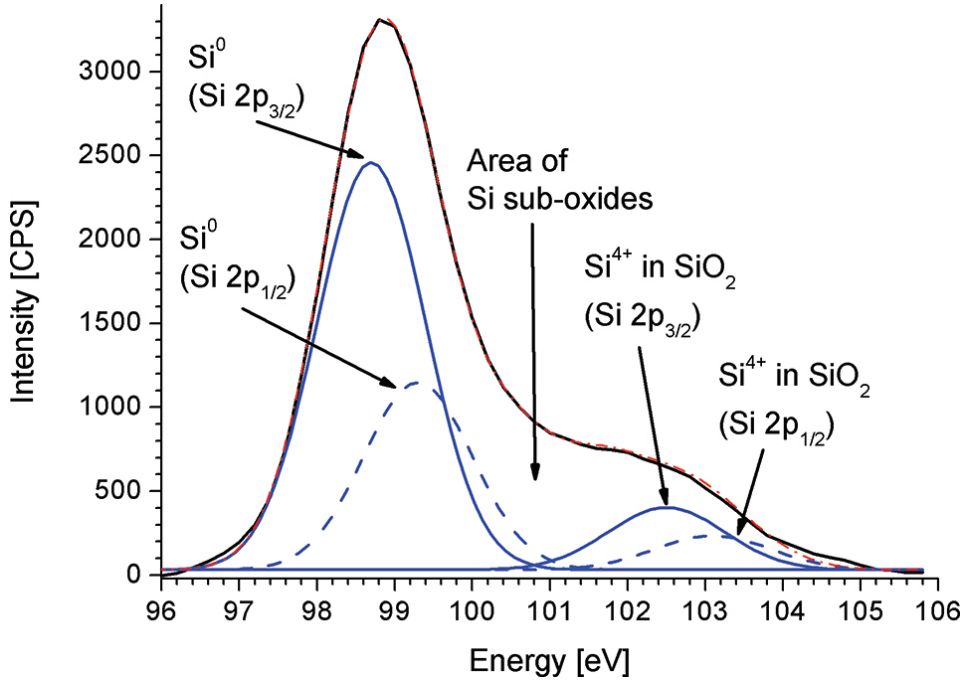

Figure 5. XPS spectrum of SRO with R_0 =1 [17].

Table 3 presents the compositions of SRO with different R_0's [17, 18]. As can be observed, the amount of elemental Si and the amount of SiO_2 monotonically increase and decrease, respectively, when decreasing the R_0. SiO_y oscillates around 43%, for R_0's higher than 3. The oscillating amount could be understood in the sense that SiO_y is in reality a combination of different stoichiometries, which vary in proportion depending on the R_0.

R_0	30	20	10	3	1
% Si	2	3	11	20	72
% SiO_y	43	47	40	46	16
% SiO_2	55	50	49	34	12

Table 3. Composition of SRO with different R_0s.

From **Table 3**, it is possible to make a fit of the monotonically varying data (Si and SiO_2). For the fit is considered that $R_0 = 0$ means 100% elemental Si, and that 0% elemental Si is obtained by $R_0 = 100$ (no Si-ncs are observed from $R_0 = 30$ [17]). From the fitting curves, it is possible to calculate the curve for SiO_y as 100 - %Si - %SiO_2. All calculated curves are shown in **Figure 6**.

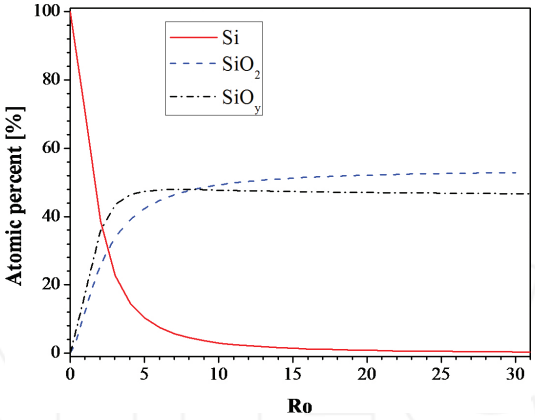

Figure 6. Calculated curves for %Si, %SiO_2, and %SiO_y, obtained by fitting measured data.

For R_0's below 8, the amount of SiO_y is larger than the amount of SiO_2. This is caused by the high Si excess. At larger R_0's, the amount of SiO_2 is larger than the one of SiO_y, nevertheless, the amounts are almost constant (vary linearly with R_0, with a small slope) at R_0's over 20, when the amount of elemental Si is close to zero. Following this tendency, the amount of SiO_y is not zero even at $R_0 = 100$ (the proportion is 44% SiO_y by 56% SiO_2). This result implies that the oxides obtained by LPCVD are in a large percentage non-stoichiometric, even at large R_0's. This nature of the oxides may mean a large number of defects, many of them being luminescent, as will be made clear in Section 6.

For our CVD system, one can write the chemical reaction as

$$SiH_4 + (2+x) * N_2O \rightarrow SiO_x + 2H_2O + (2+x) * N_2 \tag{5}$$

where

$$SiO_x = a * Si + b * SiO_y + c * SiO_2 \tag{6}$$

with a, b, and c being the atomic proportions of the different phases ($a + b + c = 1$).

It is worthy to mention that certain amount of nitrogen is incorporated in SiO_x during the deposition, but it may be of maximum 1%. Lower amounts of nitrogen are presented in samples of smaller R_0's [19]. These amounts do not change the material structurally, but may enhance its luminescence [20, 21].

It is also important to know the form how elemental Si is present in the samples. Through transmission electron microscopy (TEM) studies, it has been possible to evidence Si-ncs in samples with R_0's below 20. By larger R_0's, Si is in amorphous state or dispersed in the oxide matrix. **Figure 7** shows a plot of the sizes of the Si-ncs versus R_0 [17, 22, 23]. As can be observed,

http://dx.doi.org/10.5772/63012

the Si-nc size decreases almost linearly with the increasing of R_0, for R_0's above 3. SRO with R_0 = 1 is closer to semi-insulating polysilicon (SIPOS), presenting much bigger grains.

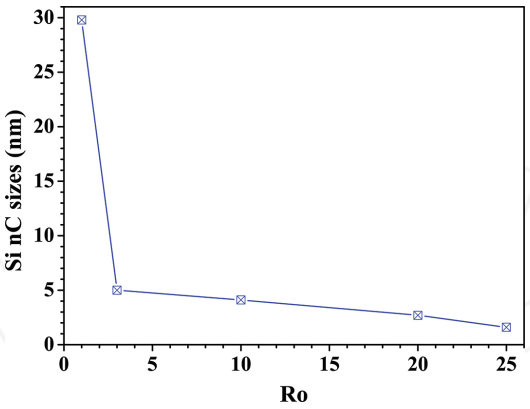

Figure 7. Si-nC sizes depending on R_0.

5. Electrical characteristics

Figure 8 shows the current density (J) as a function of the electric field (E), which it is defined as the ratio of applied voltage (V) and the thickness of the SRO film (t_{SRO}). This J-E behavior corresponds to LEC with a single layer of SRO. All LECs are forwardly biased (accumulation mode) considering the substrate as reference.

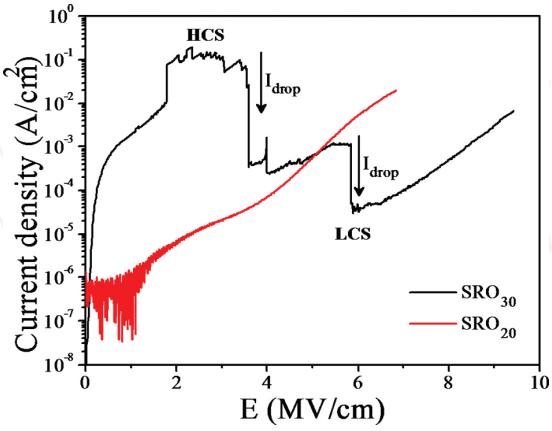

Figure 8. J-E curve of SRO_{30} and SRO_{20}-based LECs. SRO films thermally annealed at 1100°C.

As we can see, the presence of defects including the Si-nps, either crystalline or amorphous, and their density in the SRO films affect clearly the current transport when they are used in MIS devices. LEC with SRO_{30} films show a high current state (HCS) at low electric fields, and then after the applied voltage increases, the current is switched to a low conduction state (LCS), as shown in **Figure 8**. The switching from the HCS to LCS shown by SRO_{30}-based devices was observed by our group before and for both forward and reverse bias [24–28]. That effect was related to the annihilation of conductive paths created by adjacent stable Si-nps and unstable silicon nanoclusters (Si-ncls) through structural changes and by the possible creation of defects (breaking off Si-Si bonds) [24, 25, 27]. Recent studies regarding the same electrical switching in SRO films was observed and related with a conductive filament [29–32]. The conductance switching behavior observed in that SRO films was explained also by structural changes through an electroforming process. In fact, the structural changes in the conductive filament was analyzed by in situ imaging TEM analysis, showing that the conductance switch is related with a crystallization and an amorphization process of Si-nps that creates the conductive filament [30]. These observations are in agreement with our asseverations about the conductance switching observed in our SRO_{30}-based LECs [24].

In the HCS regime, current jumps and drops, which are observed independently of the temperature of annealing, have been related to the creation and annihilation of the preferential conductive paths and with the appearing or disappearing of electroluminescent spots (EL dots) on the LEC surface [24, 25, 27, 28]. A clear correlation between current jumps/drops and EL dots appearing/disappearing was observed [27]. Once the current fluctuations disappear, through an electrical annealing, the current behavior stabilizes, as reported in [24, 28].

On the other hand, the electrical behavior of most of LECs with SRO_{20} films does not show current fluctuations. This effect has been related with the presence of well-separated and crystalline silicon nanoparticles (or Si-ncs) and mainly on the density of Si-nps [28]. The Si-nps density estimated from energy-filtered transmission electron microscopy (EFTEM) images of SRO_{20} films thermally annealed at 1100°C is ~2.46×10^{12} cm^{-2}, about twice the Si-nps density in SRO_{30} with ~1.1×10^{12} cm^{-2} [27]. Therefore, a uniform network of conductive paths becomes possible as the Si-nps density increases, allowing a uniform charge flow through the whole capacitor area. Meanwhile, as the Si-nps density decreases (SRO_{30} films), the distance between them increases reducing the amount of available paths, with a resulting set of discrete and preferential conductive paths within the oxide.

Basically, there are four main mechanisms known to contribute in the carrier transport through a Si-rich oxide layer, including the direct tunneling, Fowler Nordheim tunneling (F-N), Poole-Frenkel (P-F) and the trap-assisted tunneling (TAT) [33–37]. It has been found that the TAT conduction mechanism predominates in our SRO_{30}-based LECs, where the trap energy (ϕ_t) was estimated at about 1.99 eV [28]. This implies that traps, which are placed at ~2 eV below the conduction band, would be assisting the tunneling event. On the other hand, the P-F tunneling was found as the charge transport in the SRO_{20}-based LECs. A relative permittivity (ε_r) value of 9.16 was obtained from the P-F fit, closer to the relative permittivity of silicon (ε_{Si} = 11.9), similar to other reports [36]. Relatively high permittivity values are a good indication of the large amount of silicon present as Si-nps within our SRO_{20} films. Moreover, it was found

http://dx.doi.org/10.5772/63012

that the Si-nc size obtained through a relation between size and permittivity (obtained by P-F fit) is very close to that measured by high-resolution transmission electron microscopy (HRTEM) [28].

6. Electro-optical characteristics

6.1. Single layer

6.1.1. Photoluminescence

PL spectra of annealed films from R_0 = 5 to R_0 = 50 are depicted in **Figure 9**. After annealing, all SRO samples present a main emission from ~600 to 850 nm and a negligible emission for some samples from ~380 to 500 nm. The emission intensity increases when the silicon excess decrease until a maximum of R_0 = 30 and then the PL intensity decreases until it practically disappear.

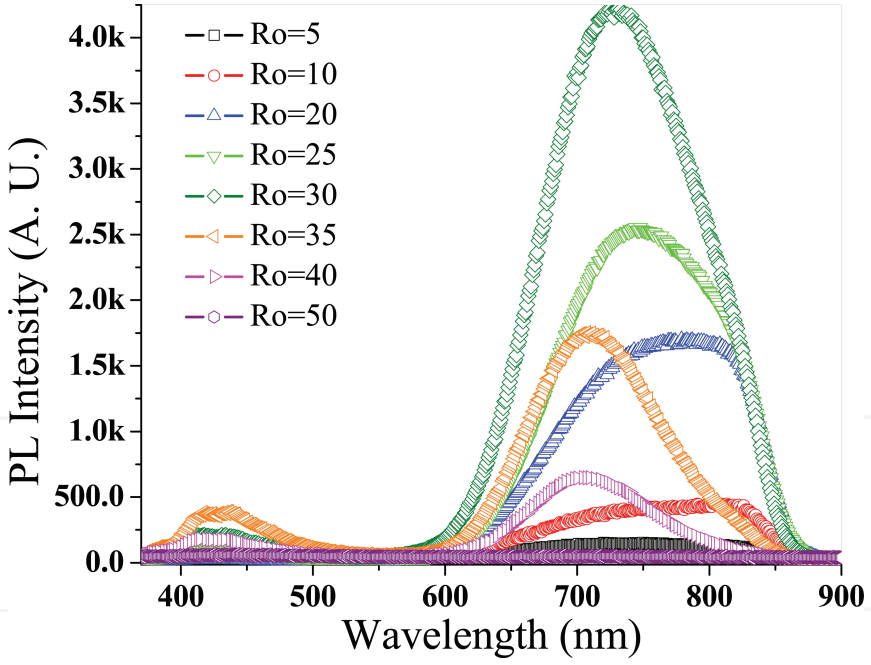

Figure 9. Photoluminescence of annealed SRO films with R_0 from 5 to 50.

As can be observed, the PL emission exhibits a shape dependence on the silicon excess, which could indicate different emission mechanism. Because of this, the multi-Gaussian deconvolution of PL spectra was performed for some annealed samples, and the set of band positions

have been determined (**Figure 10**). Each spectrum can be well fitted to a superposition of three Gaussian distributions: a main band (1) and two shoulders (2 and 3). Fit peaks are centered at (1) 710–730, (2) 780–790, and (3) 820 nm with FWHM of (1) 50–60, (2) 20–29, and (3) 18 nm, respectively.

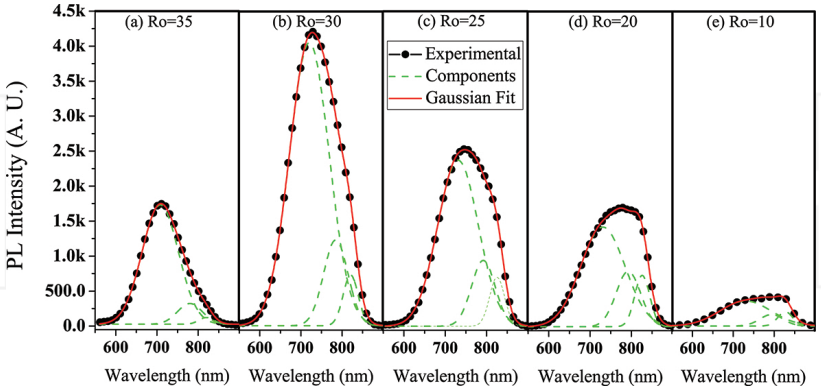

Figure 10. PL spectra and fits from SRO films with different silicon excess. Symbols are experimental data, lines are the Gaussian fits and dash lines are distributions.

Peak position and intensity vary according to the silicon excess, as shown in **Figure 11**. There is a blue wavelength shift for all components when the silicon excess decreases (except for R_0 = 5), see **Figure 11(a)**. The main contribution of the luminescence is the peak 1 that increases rapidly as R_0 increases until R_0 = 30 and then decreases, as can be seen in **Figure 11(b)**. While peaks 2 and 3 slightly increase when R_0 increases, due to this, samples with R_0 < 25 shows a shoulder in the near infrared region (NIR). Since there are different components that change with silicon excess, it can be assumed that PL emission is related with at least three different types of emission centers (or emission mechanism).

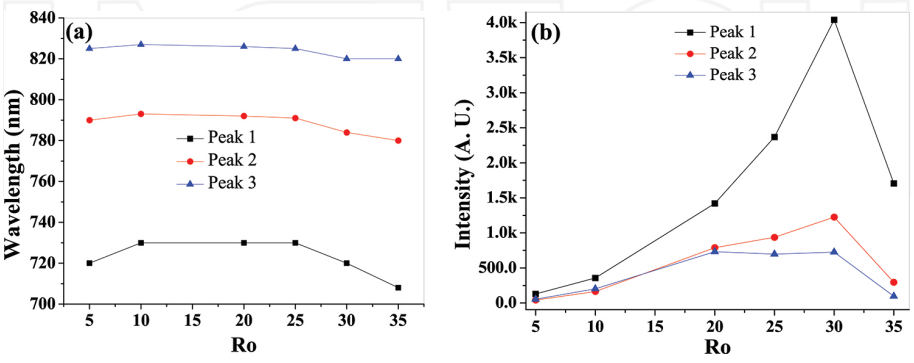

Figure 11. (a) Position and (b) intensity of the fit distributions for different silicon excess.

http://dx.doi.org/10.5772/63012

6.1.2. Cathodoluminescence

CL spectra from SRO films with different silicon excess are depicted in **Figure 12(a)**. The CL spectra of SRO with thermal treatment consist of a broad emission in the visible and NIR from ~400 to 850 nm. After annealing, intensity of the blue band at ~460 nm increases with increasing the R_0. On the other hand, the intensity of the red-NIR CL band seems to have a maximum for $R_0 = 20$.

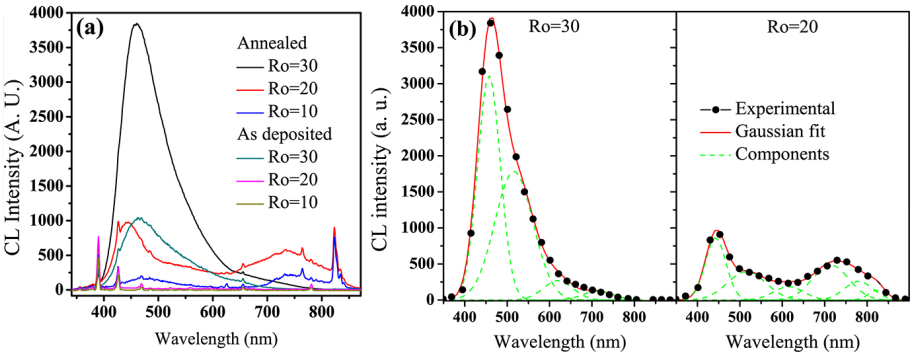

Figure 12. (a) Cathodoluminescence spectra from SRO films with different silicon excess. (b) Gaussian fit of CL experimental spectrum, the best fit requires four distributions for $R_0 = 30$ and six distributions for $R_0 = 20$.

As CL emission has asymmetrical shape for all SRO samples, it can be assumed that CL emission is also due to different luminescent centers. Hence, multi-Gaussian deconvolution of CL spectra was also obtained, shown in **Figure 12(b)**. The best fit of CL spectra requires four and six components for $R_0 = 30$ and 20, respectively. Peaks (or distributions) were obtained at about 460, 522, 643, and 714 nm for $R_0 = 30$ and 447, 541, 645, 714, 780, and 823 nm for $R_0 = 20$. Peaks obtained at 714, 780, and 823 nm in CL are centered in the same position than distributions obtained from PL spectrum in $R_0 = 20$. Furthermore, peak at 714 nm was obtained for Gaussian fit, in PL and CL in $R_0 = 30$. Then, the red emission of the CL emission can be ascribed to the same PL emissive centers. PL distributions in higher wavelength are not observed in CL due to either destruction of the emissive centers or inefficient emission from low-energy emissive centers [38]. The latter one could occur increasingly because cathode-excited electrons acquire so high energy that they arrive to the higher emissive positions where they emit in the blue region (higher energy); however, almost none of the excited electrons reach that with lower energy; then, the red emission is not likely to occur in CL. Therefore, there could be several different kinds of emission traps located at different energy levels in SRO.

Depending on the emission wavelength, multiple luminescence centers have been reported in SiO_2 films. Luminescent emission at 460 nm (2.7 eV), 520 nm (2.4 eV) and 650 nm (1.9 eV) nm are mainly related to defects such as oxygen deficiency-related centers (ODC) or oxygen vacancies [39–41], *E'δ* defect or peroxide radical [42] and non-bridging oxygen hole centers (NBOHC) [40, 41, 43], respectively. Since CL and PL measurements have shown luminescent peaks (or distributions) close to those wavelengths, such defects could be inside the SRO films.

6.1.3. Electroluminescence

Figure 13 shows the electroluminescence spectra from the SRO-based LECs. Blue electroluminescence is observed in the SRO_{30} film, as observed in **Figure 13(a)**. Nevertheless, this blue EL in whole area of LECs is obtained only after the current drop. The main EL peak remains at 468 nm even for different thermal annealing temperatures [28]. A long spectral shift, blue shift, of almost ~227 nm has been observed between the EL and PL band of the SRO_{30} films. Devices with SRO_{20} films emit a broad EL spectrum in the red region (713 nm), as observed in **Figure 13(b)**. An additional EL peak of low intensity is also observed at 468 nm. There exists also a blue shift of the EL spectra with respect to PL spectrum in SRO_{20} films. Nevertheless, both EL and PL spectra in SRO_{20} films appear in the red region, which could indicate that the same luminescent centers are involved. Images of the blue and red LECs are shown in the insets of the **Figure 13**. As we can see, intense EL is emitted in the whole area of the LEC devices.

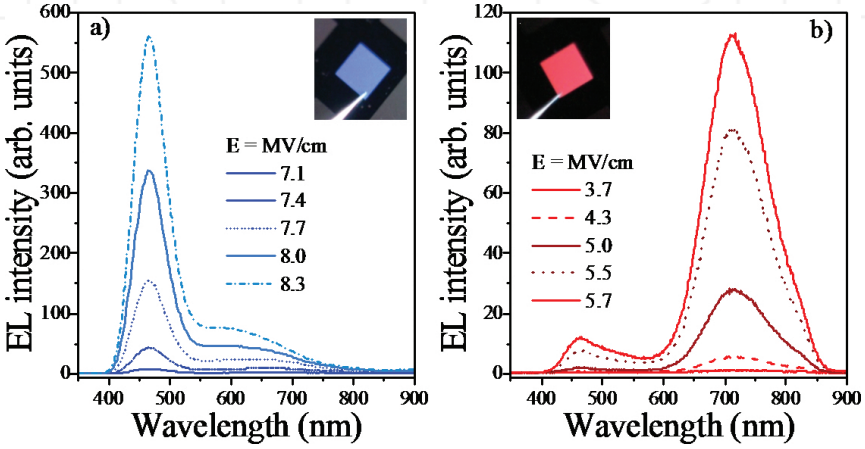

Figure 13. EL spectra of (a) SRO_{30} and (b) SRO_{20} based LECs biased at different electric fields. Insets show images of each SRO-based LECs.

The spectral shift between PL and EL has been reported before and it has been explained according to three different mechanisms [35, 44, 45]. Our experimental results have suggested that the red EL observed in SRO_{20} films can be related with the combination of some surface defect on the Si-ncs, while the blue EL in SRO_{30} devices is consistent with the defect emission which could be intrinsically present or generated by electric field within the SRO matrix [28].

6.2. Multilayer

6.2.1. Photoluminescence

Multilayer structures were fabricated in order to improve the optical properties of the SRO films. Two samples were obtained, one of those is a combination of low silicon excess ($R_0 = 25$) and high silicon excess ($R_0 = 5$) and the second one is a combination of $R_0 = 25$ and $R_0 = 10$.

http://dx.doi.org/10.5772/63012

PL spectra of annealed multilayers and single layer are shown in **Figure 14(a)**. As can be seen the intensity emission is improved in the multilayer samples, where multilayer SRO_{10}/SRO_{25} (ML-10/25) is the most intense. In order to obtain the components of every layer, the multi-Gaussian deconvolution of PL spectra was also obtained. **Figure 14(b)** and **(c)** shows the position and the intensity of the three peaks obtained from the Gaussian deconvolution. There is a blue-shift wavelength for the three peaks that can be due to the participation of high silicon excess (R_0 = 5 or 10) on the PL. The intensity improvement could be due to the three components together, peak 1 is from R_0 = 25 and the improvement of peaks 2 and 3 comes from high silicon excess (R_0 = 5 or 10).

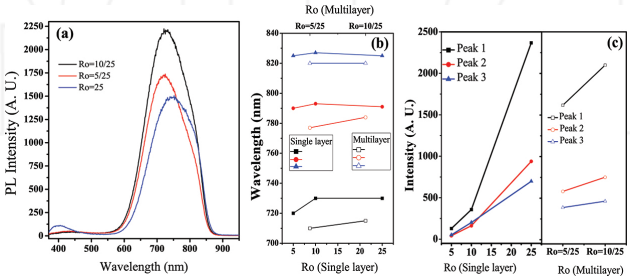

Figure 14. (a) Photoluminescence of annealed multilayer SRO films (R_0 = 10/25 and R_0 = 5/25) and a single layer of R_0 = 25. (b) Position and (c) intensity of the fit distribution for single layer (R_0 = 5, 10, and 25) and multilayers.

6.2.2. Electroluminescence

Figure 15 shows a scheme of the multilayered structure fabricated with its dimensional characteristics (left side), and a TEM image of the structure, which exposes the layers composing the SRO multilayer (right side). The goal of this structure is to improve the electro-optical properties of the LECs. In this multilayer, the luminescent properties of three layers with low silicon excess (SRO_{25}) are combined with four conducting layers (SRO_5).

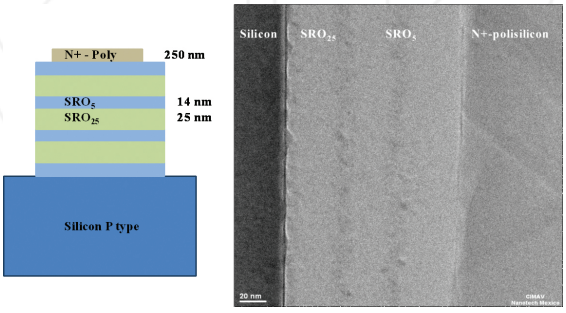

Figure 15. Scheme of a light emitter capacitor with a multilayered SRO films (left side) and a TEM image of the SRO nanometric multilayer (right side).

The electroluminescence in this ML-SRO-based LEC is observed at forwardly bias considering the substrate as reference. A broad band with the main peak at about 600 nm is observed with E = 3.7 MV/cm, as we can see in **Figure 16**. As the voltage increases, the spectrum is divided in two. One peak at 680 nm and other at 450 nm, the blue peak increases to higher intensity than the red one. Apparently, SRO_5 layers increase the conductivity across the structure and SRO_{25} layers produces the emission. The spectrum behavior shown in our samples have been observed in other reports [26].

However, the electric field needed to turn on the emission on an ML-SRO-based LEC is lower than an LEC of single layer (see **Figures 13** and **16**). This proves that the electro-optical properties of a ML-SRO-based LEC are improved, thereby the conductivity of the structure is increased by layers of high silicon excess, and luminescence response is conserved using layers of high R_0.

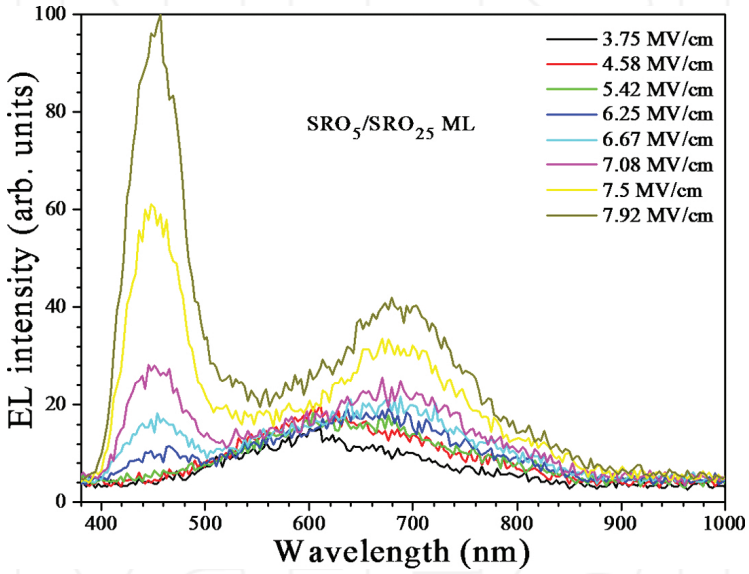

Figure 16. EL spectra of a multilayered SRO_5/SRO_{25}-based LEC under different electric fields.

7. Conclusion

In this chapter, details of a homemade hot-wall LPCVD system were presented. Also, important aspects of how to obtain SRO in a reliable and repetitive form were addressed. We show that in our system, it is possible to obtain single layers with variable silicon excess, and also good quality multilayered structures of nanometric layers. The structural, electrical, and luminescent characteristics of single- and multilayered structures were reviewed and discussed.

Acknowledgements

Authors recognize the financial support of the CONACYT, particularly, J. Alarcón-Salazar for his grant with number 353251. Also, authors thank the microelectronic laboratory technicians Pablo Alarcon, Victor Aca, and Armando Hernández for their help during the fabrication process.

Author details

J. Alarcón-Salazar[1*], R. López-Estopier[2], E. Quiroga-González[3], A. Morales-Sánchez[4], J. Pedraza-Chávez[1], I. E. Zaldívar-Huerta[1] and M. Aceves-Mijares[1]

*Address all correspondence to: j.alarcon.sal@gmail.com

1 Electronics Department, National Institute of Astrophysics Optics and Electronics (INAOE), Puebla, México

2 Professor CONACYT – IICO-UASLP, Karakorum, San Luis Potosí, México

3 Institute of Physics, Autonomous University of Puebla, México

4 Advanced Materials Research Center (CIMAV), Monterrey, Apodaca, Nuevo León, México

References

[1] Guangzhao Ran, Hongqiang Li, and Chong Wang. On-chip silicon light source: from photonics to plasmonics. Front. Optoelectron. 2012;5(1):3–6. DOI:10.1007/s12200-012-0221-x

[2] Kingsley A. Ogudo, Diethelm Schmieder, Daniel Foty, and Lukas W. Snyman. Optical propagation and refraction in silicon complementary metal–oxide–semiconductor structures at 750 nm: toward on-chip optical links and microphotonic systems. J. Micro/Nanolith. MEMS MOEMS. 2013;12(1):013015. DOI:10.1117/1.JMM.12.1.013015

[3] A. Anopchenko, A. Marconi, F. Sgrignuoli, L. Cattoni, A. Tengattini, G. Pucker, Y. Jestin, and L. Pavesi. Electroluminescent devices based on nanosilicon multilayer structures. Phys. Status Solidi A. 2013;210(8);1525–1531. DOI:10.1002/pssa.201200957

[4] M. Aceves-Mijares, A. A. González-Fernández, R. López-Estopier, A. Luna-López, D. Berman-Mendoza, A. Morales, C. Falcony, C. Domínguez, and R. Murphy-Arteaga. On

the origin of light emission in silicon rich oxide obtained by low-pressure chemical vapor deposition. J. Nanomater. 2012;2012:890701. DOI:10.1155/2012/890701

[5] A. A. González-Fernández, J. Juvert, M. Aceves-Mijares, C. Domínguez. Monolithic integration of a silicon-based photonic transceiver in a CMOS process. IEEE Photonics J. 2016;8(1):7900213. DOI:10.1109/JPHOT.2015.2505144

[6] A. Morales, J. Barreto, C. Domínguez, M. Riera, M. Aceves, and J. Carrillo. Comparative study between silicon-rich oxide films obtained by LPCVD and PECVD. Phys. E Low Dimens. Syst. Nanostruct. 2007;38(1–2):54–58. DOI:10.1016/j.physe.2006.12.056

[7] D. Dong, E. A. Irene, and D. R. Young. Preparation and some properties of chemically vapor-deposited Si-rich SiO and SigN, films. J. Electrochem. Soc. 1978;125(5):819–823. DOI:10.1149/1.2131555

[8] M. Aceves, L. A. Hernandez, and R. Murphy. Applying statistics to find the causes of variability of aluminum deposition: a case study. IEEE Trans. Semicond. Manuf. 1992;5(2):165–167. DOI:10.1109/66.136280

[9] H. O. Pierson. Handbook of chemical vapor deposition (CVD): Principles, technology, and applications. 2nd ed. New Jersey, USA: Noyes Publications; 1999.

[10] Hwaiyu Geng. Chemical vapor deposition. In: Hwaiyu Geng, editor. Semiconductor manufacturing handbook. 1st ed. New York, USA: McGraw-Hill Handbooks; 2005.

[11] Y.-P. Zhao, J. T. Drotar, G.-C. Wang, and T.-M. Lu. Morphology transition during low-pressure chemical vapor deposition. Phys. Rev. Lett. 2001;87(13)1–4. DOI:10.1103/PhysRevLett.87.136102

[12] F. Verpoort, P. Persoon, L. Fiermans, G. Dedoncker, and L. Verdonck. SiO2/Si(100)model support with AES and XPS in combination with MLCFA. J. Chem. Soc., Faraday Trans. 1997;93(19):3555. DOI:10.1039/A702279D

[13] G. Hollinger and F. J. Himpsel. Probing the transition layer at the SiO2-Si interface using core level photoemission. Appl. Phys. Lett. 1984;44(1):93–95. DOI:10.1063/1.94565

[14] F. J. Grundthaner, P. J. Grundthaner, R. P. Vasquez, B. F. Lewis, and J. Maserjian. High-resolution X-ray photoelectron spectroscopy as a probe of local atomic structure: Application to amorphous SiO_2 and the Si-SiO_2 interface. Phys. Rev. Lett. 1979;43(22):1683. DOI:10.1103/PhysRevLett.43.1683

[15] P. J. Grundthaner, M. H. Hecht, F. J. Grundthaner, and N. M. Johnson. The localization and crystallographic dependence of Si suboxide species at the SiO2/Si interface. J. Appl. Phys. 1987;61(2):629. DOI:10.1063/1.338215

[16] K. Hirose, H. Nohira, K. Azuma, and T. Hattori. Photoelectron spectroscopy studies of SiO2/Si interfaces. Prog. Surf. Sci. 2007;82(1):3. DOI:10.1016/j.progsurf.2006.10.001

[17] E. Quiroga-González, W. Bensch, M. Aceves-Mijares, Z. Yu, R. López-Estopier, and K. Monfil-Leyva. On the photoluminescence of multilayer arrays of silicon rich oxide with

high silicon content prepared by low pressure chemical vapor deposition. Thin Solid Films. 2011;519:8030–8036. DOI:10.1016/j.tsf.2011.06.020

[18] R. López-Estopier, M. Aceves-Mijares, and C. Falcony. Cathodo- and photo-luminescence of silicon rich oxide films obtained by LPCVD, cathodoluminescence. In: Naoki Yamamoto, editor. Chathodoluminescence. InTech; Shanghai China; 2012. DOI: 10.5772/34888

[19] E. Quiroga, W. Bensch, Z. Yu, M. Aceves, R. A. De Souza, M. Martin, V. Zaporojtchenko, and F. Faupel. Structural characteristics of a multilayer of silicon rich oxide (SRO) with high Si content prepared by LPCVD. Phys. Stat. Sol. A. 2009;206(2):263–269. DOI: 10.1002/pssa.200824365

[20] R. López-Estopier, M. Aceves-Mijares, and C. Falcony. Photoluminescence of silicon rich oxide films with different silicon excess and nitrogen content. In: 3rd International Conference on Electrical and Electronics Engineering (ICEEE); Mexico City. IEEE; 2006. DOI:10.1109/ICEEE.2006.251868

[21] R. López-Estopier, M. Aceves-Mijares, J. Carrillo, Z. Yu, and C. Falcony. Effect of nitrogen in the photoluminescence of silicon rich oxide films prepared by LPCVD. In: 2nd International. Conference on Electrical and Electronics Engineering (ICEEE) and XI Conference on Electrical Engineering (CIE); Mexico City. IEEE; 2005. p. 227–230. DOI:10.1109/ICEEE.2005.1529614

[22] E. Quiroga, W. Bensch, M. Aceves, Z. Yu, J. P. Savy, M. Haeckel, and A. Lechner. Silicon rich oxide with controlled mean size of silicon nanocrystals by deposition in multilayers. In: 10th International Conference on Ultimate Integration of Silicon; March 18–20; Aachen, Germany. IEEE; 2009. p. 349–352. DOI:10.1109/ULIS.2009.4897607

[23] J. A. Luna-López, M. Aceves-Mijares, J. Carrillo-López, and A. Morales-Sánchez. Photoconduction in silicon rich oxide films obtained by low pressure chemical vapor Deposition. J. Vac. Sci. Technol. A. 2010;28(2):170–174. DOI:10.1116/1.3276781

[24] A. Morales-Sánchez, J. Barreto, C. Domínguez, M. Aceves, and J. A. Luna-López. The mechanism of electrical annihilation of conductive paths and charge trapping in silicon-rich oxides. Nanotechnology. 2009;20(4):045201. DOI:10.1088/0957-4484/20/4/045201

[25] A. Morales-Sánchez, J. Barreto, C. Domínguez, M. Aceves-Mijares, J. A. Luna-López, M. Perálvarez, and B. Garrido. DC and AC electroluminescence in silicon nanoparticles embedded in silicon-rich oxide films. Nanotechnology. 2010;21(8):085710. DOI: 10.1088/0957-4484/21/8/085710

[26] A. A. González Fernández, M. Aceves Mijares, A. Morales Sánchez, and K. M. Leyva. Intense whole area electroluminescence from low pressure chemical vapor deposition-silicon-rich oxide based light emitting capacitors. J. Appl. Phys. 2010;108(4):043105. DOI:10.1063/1.3465335

[27] A. Morales-Sánchez, M. Aceves-Mijares, K. Monfil-Leyva, A. A. González, J. A. Luna-López, J. Carrillo, C. Domínguez, J. Barreto, and F. J. Flores-Gracia. Strong blue and red

luminescence in silicon nanoparticles based light emitting capacitors. Appl. Phys. Lett. 2011;99(17):1711102. DOI:10.1063/1.3655997

[28] L. Palacios Huerta, S. A. Cabañas Tay, J.-A. Luna López, M. Aceves, A. Coyopol, and A. Morales-Sánchez. Effect of the structure on luminescent characteristics of SRO-based light emitting capacitors. Nanotechnology. 2015;26(39):395202. DOI: 10.1088/0957-4484/26/39/395202

[29] J. Yao, Z. Sun, L. Zhong, D. Natelson, and J. M. Tour. Resistive switches and memories from silicon oxide. Nano Lett. 2010;10(10):4105. DOI:10.1021/nl102255r

[30] J. Yao, L. Zhong, D. Natelson, and J. M. Tour. In situ imaging of the conducting filament in a silicon oxide resistive switch. Sci. Rep. 2012;2(242):1-5. DOI:10.1038/srep00242

[31] A. Mehonic, A. Vrajitoarea, S. Cueff, S. Hudziak, H. Howe, C. Labbé, R. Rizk, M. Pepper, and A. J. Kenyon. Quantum conductance in silicon oxide resistive memory devices. Sci. Rep. 2013;3:2708. DOI:10.1038/srep02708

[32] A. Mehonic, S. Cueff, M. Wojdak, S. Hudziak, C. Labbé, R. Rizk, and A. Kenyon. Electrically tailored resistance switching in silicon oxide. Nanotechnology. 2012;23(45): 455201. DOI:10.1088/0957-4484/23/45/455201

[33] B. H. Lai, C. H. Cheng, and G. R. Lin. Multicolor ITO/SiOx/P-Si/Al light emitting diodes with improved emission efficiency by small Si quantum dots. IEEE J. Quantum Electron. 2011;47(5):698. DOI:10.1109/JQE.2011.2109699

[34] S. Cueff, S. Labbé, O. Jambois, Y. Berencén, A. J. Kenyon, B. Garrido, and R. Rizk. Structural factors impacting carrier transport and electroluminescence from Si nanocluster-sensitized Er ions. Opt. Express. 2012;20(20):22490. DOI:10.1364/OE.20.022490

[35] B. H. Lai, C. H. Cheng, and G. R. Lin. Electroluminescent wavelength shift of Si-rich SiOx based blue and green MOSLEDs induced by O/Si composition Si-QD size variations. Opt. Mater. Express. 2013;3(2):166. DOI:10.1364/OME.3.000166

[36] J. M. Ramírez, Y. Berencén, L. López-Conesa, J. M. Rebled, F. Peiró, and B. Garrido. Carrier transport and electroluminescence efficiency of erbium-doped silicon nancrystals superlattices. Appl. Phys. Lett. 2013;103:081102. DOI:10.1063/1.4818758

[37] R. Perera, A. Ikeda, R. Hattori, and Y. Kuroki. Trap assisted leakage current conduction in thin silicon oxynitride films grown by rapid thermal oxidation combined microwave excited plasma nitridation. Microelectron. Eng. 2003;65(4):357–370. DOI:10.1016/S0167-9317(02)01025-0

[38] A. N. Trukhin., H. J. Fitting, T. Barfels, and V. Czarnowski. Cathodoluminescence and IR absorption of oxygen deficient silica – influence of hydrogen treatment. J. Non-Cryst. Solids. 1999;260(1–2):132–140. DOI:10.1016/S0022-3093(99)00558-X

[39] M. Cervera, M. J. Hernández, P. Rodríguez, J. Piqueras, M. Avella, M. A. González, and J. Jimenez. Blue-cathodoluminescent layers synthesis by high-dose N+, C+ and B+ SiO_2 implantation. J. Lumin. 2006;117(1):95–100. DOI:10.1016/j.jlumin.2005.03.015

[40] H. J. Fitting. Can we make silica luminescent? Opt. Mater. 2009;31(12):1891–1893. DOI: 10.1016/j.optmat.2008.07.015

[41] V. A. Gritsenko, Y. G. Shavalgin, P. A. Pundur, H. Wong, and W. M. Lau. Cathodoluminescence and photoluminescence of amorphous silicon oxynitride. Microelectron. Reliab. 1999;39(5):715–718. DOI:10.1109/ICMEL.2000.840567

[42] M. Goldberg, H. J. Fitting, and A. Trukhin. Cathodoluminescence and cathodoelectroluminescence of amorphous SiO_2 films. J. Non-Cryst. Solids. 1997;220(1):69–77. DOI: 10.1016/S0022-3093(97)00225-1

[43] H. J. Fitting, T. Barfels, and A. N. Trukhin. Cathodoluminescence of crystalline and amorphous SiO_2 and GeO_2. J. Non-Cryst. Solids. 2001;279(1):51–59. DOI:10.1016/S0022-3093(00)00348-3

[44] D. C. Wang, J. R. Chen, J. Zhu, C.-T. Lu, and M. Lu. On the spectral difference between electroluminescence and photoluminescence of Si nanocrystals: A mechanism study of electroluminescence. J. Nanopart. Res. 2013;15(11):2063. DOI:10.1007/s11051-013-2063-x

[45] D. Chen, Z. Q. Xie, Q. Wu, Y. Y. Zhao, and M. Lu. Electroluminescence of Si nanocrystals-doped SiO_2. Chin. Phys. Lett. 2007;24(8):2390. DOI:10.1088/0256-307X/24/8/064

INTECH